Hypoxic CAF studies unveil PTHrP-vitamin D-RAS axis as pivotal in the CAF

SHOICHIRO NAKAJO[1*], MAMORU UEMURA[1*], HIROSHI KUSAFUKA[1], MAO OSAKI[1], CHIKAKO KUSUNOKI[1], NOBUO TAKIGUCHI[1], MITSUNOBU TAKEDA[1], YUKI SEKIDO[1], TSUYOSHI HATA[1], ATSUSHI HAMABE[1], TAKAYUKI OGINO[1], NORIKATSU MIYOSHI[1], MITSUYOSHI TEI[2], YOSHINORI KAGAWA[3], HIROFUMI YAMAMOTO[1], YUICHIRO DOKI[1] and HIDETOSHI EGUCHI[1]

[1]Department of Gastroenterological Surgery, Graduate School of Medicine, University of Osaka, Suita, Osaka 565-0871, Japan; [2]Department of Surgery, Osaka Rosai Hospital, Sakai, Osaka 591-8025, Japan; [3]Department of Gastroenterological Surgery, Osaka General Medical Center, Osaka, Osaka 558-8558, Japan

Received May 22, 2025; Accepted December 8, 2025

DOI: 10.3892/or.2026.9114

Abstract. Cancer-associated fibroblasts (CAFs) play critical roles in the tumor microenvironment (TME); however, their characteristics under hypoxic conditions remain incompletely understood. The aim of the present study was to investigate the properties of hypoxic CAFs and identify their regulatory factors in colorectal cancer (CRC). CAFs cultured under normoxic and hypoxic conditions were analyzed using proliferation assays, co-culture experiments, shotgun proteomics and single-cell RNA sequencing. Clinical specimens were evaluated immunohistochemically using the desmoplastic reaction (DR) classification. In addition, the generalizability of the findings was validated by correlation analyses using The Cancer Genome Atlas database. Hypoxic CAFs showed enhanced proliferative capacity, and their conditioned medium promoted migration and chemoresistance in CRC cells. Shotgun proteomics revealed a significant increase in vitamin D-binding protein in the conditioned media of hypoxic CAFs, while single-cell RNA sequencing showed enrichment of genes related to bone metabolism and the phosphoinositide 3-kinase-AKT signaling pathway. Treatment of normal fibroblasts (NFs) with parathyroid hormone-related protein (PTHrP) induced CAF-like phenotypes, whereas treatment of CAFs with vitamin D led to morphological changes toward a NF-like appearance. In clinical samples, the immature DR subtype, associated with poor prognosis, exhibited increased expression of the hypoxia marker hypoxia-inducible factor-1α, periostin and PTHrP, along with a significant association with Kirsten rat sarcoma viral oncogene homolog (KRAS) mutations. Furthermore, a strong positive correlation was observed between the copy numbers of PTHrP and KRAS across multiple cancer types, including CRC. These findings suggest that the PTHrP-vitamin D-rat sarcoma oncogene (RAS) axis functions as an important regulatory mechanism in hypoxic CAFs. PTHrP and vitamin D may influence each other's activity, and this axis may contribute to tumor progression within the TME. Therefore, the PTHrP-vitamin D-RAS axis could serve as a potential therapeutic target.

Correspondence to: Dr Mamoru Uemura, Department of Gastroenterological Surgery, Graduate School of Medicine, University of Osaka, 2-2 E2, Suita, Osaka 565-0871, Japan
E-mail: muemura@gesurg.med.osaka-u.ac.jp

*Contributed equally

Abbreviations: AKT, protein kinase B; CAF, cancer-associated fibroblast; CNV, copy number variation; CRC, colorectal cancer; DBP, vitamin D-binding protein; DEG, differentially expressed gene; DMEM, Dulbecco's Modified Eagle Medium; DMSO, dimethyl sulfoxide; DR, desmoplastic reaction; EpCAM, epithelial cell adhesion molecule; FBS, fetal bovine serum; GO, Gene Ontology; HIF-1α, hypoxia-inducible factor 1-alpha; KRAS, Kirsten rat sarcoma viral oncogene homolog; NCBI, National Center for Biotechnology Information; NF, normal fibroblast; PBS, phosphate-buffered saline; PI3K-AKT, phosphoinositide 3-kinase-AKT signaling pathway; PTH, parathyroid hormone; PTHrP, PTH-related protein; RAS, rat sarcoma oncogene; RRID, research resource identifier; TCGA, The Cancer Genome Atlas; TME, tumor microenvironment; VDR, vitamin D receptor; αSMA, alpha-smooth muscle actin

Key words: CAF, hypoxia, CRC, PTHrP, RAS, vitamin D

Introduction

Cancer-associated fibroblasts (CAFs) exhibit fibroblast-like morphology and are known to exert both tumor-promoting and -suppressing effects (1). CAFs are located in the peritumoral area and constitute one of the most crucial components of the tumor microenvironment (TME) (2). They play vital roles in tumor growth, invasion and metastasis (3,4). In addition to the significant impact of CAFs on cancer cells, cancer cells also influence CAFs, highlighting the importance of their mutual crosstalk in understanding tumor biology (5).

The desmoplastic reaction (DR) classification has been reported as a stromal evaluation index associated with

prognosis in resected colorectal cancer (CRC) samples (6). DR refers to the fibrotic response generated by fibroblasts surrounding the tumor, and this stromal component is known to express CAF markers (7). In CRC, DR is classified into three categories: i) Immature; ii) intermediate; and iii) mature; and serves as a prognostic predictor (8).

Since CAFs form cancer stroma and interact closely with cancer cells, evaluating CAF activity and cancer stromal status through DR classification appears crucial. The immature classification in DR is known to indicate poor prognosis in CRC (9). Periostin is a key gene in the fibrogenic response of the stroma in CRC, and periostin is reported to be positively associated with the immature classification in DR (10). DR and periostin expression are considered to play an important role in the evaluation of CAFs in clinical specimens.

The hypoxic environment within tumors affects key areas of cancer biology, including cellular invasion, metastasis and the regulation of cell death (11). Reported evidence indicated that gene expression patterns associated with hypoxia are linked to unfavorable outcomes in human malignancies (12). A previous study (13) by the authors revealed that CRC liver metastases show a progressive reduction in vascular density and become increasingly hypoxic toward the center of the metastases. Using microarray analysis of cells from the central region of the metastases, several novel hypoxia-inducible genes including adrenomedullin (14), procollagen-lysine, 2-oxoglutarate 5-dioxygenase 2 (15), ephrin-A1 (16,17), secretoglobin family 2A member 1 (18) and aldolase A (19) were identified to be associated with CRC prognosis (13). In pancreatic cancer (PCa), hypoxia in the TME has been reported to enhance cytokine-induced inflammatory CAF phenotype and promote tumor growth (20).

While hypoxia is known to enhance malignant tumor behavior, the specific roles and functional characteristics of CAFs under hypoxic conditions in CRC remain largely unclear. The aim of the current study is to elucidate the effects of hypoxia, a fundamental condition in solid tumors, on CAFs and to identify key factors involved in hypoxic CAFs. The findings will contribute to a deeper understanding of the interaction between CAFs and cancer cells.

Materials and methods

Patient selection criteria and specimen collection. Patients who underwent surgical procedures at The University of Osaka Hospital between October 2023 and May 2024 and were diagnosed with CRC according to the guidelines of the Japanese Society for Cancer of the Colon and Rectum (21) were considered for inclusion. Exclusion criteria included inflammatory bowel disease and familial adenomatous polyposis. No exclusions were made based on age or disease stage. All cases that underwent surgery during the specified period and were evaluated by DR classification were included in the study. A total of 59 CRC tissue samples were included using opportunistic sampling based on the availability of cases meeting the inclusion criteria; the sample size was not determined by formal power calculation. The study cohort consisted of 26 males and 33 females, with a median age of 73 years (range: 40-88 years). All patients received a definitive diagnosis of CRC. Clinicopathological classification was determined using the criteria of the Japanese Society for Cancer of the Colon and Rectum. After surgery, patients with lymph node metastasis generally received adjuvant chemotherapy. Collected samples were immersed in 10% buffered formalin and fixed overnight at 4˚C, then dehydrated through a graded ethanol series and embedded in paraffin.

Ethics approval and patient consent. The current study was approved by the ethics committee of the Graduate School of Medicine, University of Osaka (approval nos. 15144 and 19020; Suita, Japan). Written informed consent was obtained from all participants prior to inclusion in the study. The study protocol conformed to the ethical guidelines of the 1975 Declaration of Helsinki.

Clinical sample collection and histological evaluation. Between October 2023 and May 2024, 59 CRC tissue samples were collected during surgeries performed at the Department of Gastroenterological Surgery, University of Osaka. Samples were formalin-fixed at 4˚C overnight, processed through graded ethanol and embedded in paraffin. A pathologist blinded to the clinical outcomes classified 16 cases as having immature DR and 43 as mature based on established histological criteria.

Colon fibroblasts. CAFs and normal fibroblasts (NFs) were isolated from tumor and adjacent normal tissues, respectively, immediately after CRC resection. To prevent cross-contamination, separate surgical blades were used for each tissue type. Tissue fragments underwent enzymatic digestion with collagenase, and the resulting cell pellet was suspended in Dulbecco's Modified Eagle Medium (DMEM; Sigma-Aldrich; Merck KGaA; RRID:SCR_001905) with antibiotics. Cells were seeded in 6-well plates with DMEM supplemented with 10% fetal bovine serum (FBS; Gibco; Thermo Fisher Scientific, Inc.; RRID:SCR_008452) and cultured at 37˚C with 5% CO_2.

Cell culture conditions. CAFs and NFs were cultured in DMEM supplemented with 10% FBS under normoxic (37˚C, 5% CO_2) and hypoxic (37˚C, 1% O_2) conditions. The human CRC cell lines HT29 (RRID: CVCL_0320), HCT116 (RRID: CVCL_0291) and RKO (RRID: CVCL_0504) were obtained from the American Type Culture Collection and authenticated using short tandem repeat profiling within 6 months of experimental use. Cell lines were routinely tested for mycoplasma contamination using polymerase chain reaction and were maintained in DMEM supplemented with 10% FBS under the same conditions as fibroblasts.

Immunofluorescence staining. Cells were cultured in 96-well plates for 24 h, fixed with 4% paraformaldehyde at room temperature (RT) for 15 min and treated with Triton X-100 and 5% bovine serum albumin (MilliporeSigma) at RT for 10 min. Subsequently, cells were washed twice with phosphate-buffered saline (PBS), and primary antibodies including anti-α-smooth muscle actin (α-SMA; 1:400; cat. no. 19245; Cell Signaling Technology, Inc.; RRID: AB_2734735), anti-hypoxia-inducible factor-1α (HIF-1α; 1:500; cat. no. ab51608; Abcam; RRID: AB_880418) and anti-epithelial cell adhesion molecule (EpCAM; 1:500; cat. no. 2929; Cell Signaling Technology,

Inc.; RRID: AB_2098834) were applied. Cells were incubated at RT for 1 h, washed twice with PBS and incubated with Alexa Fluor 647 anti-rabbit IgG secondary antibody (1:500; cat. no. 4414; Cell Signaling Technology, Inc.; RRID: AB_10694544) for 30 min. After washing with PBS, cells were counterstained with 4',6-diamidino-2-phenylindole (1 μg/ml) and visualized using a confocal microscope.

Immunohistochemical staining. Immunohistochemistry was performed as previously described (10,11). Primary antibodies used included anti-HIF-1α (1:200), anti-periostin (1:400; cat. no. 20302; Cell Signaling Technology, Inc.; RRID: AB_2798819), anti-parathyroid hormone-related protein (PTHrP; 1:200; cat. no. 10817-1-AP; Proteintech Group, Inc.; RRID: AB_2174535) and anti-vitamin D receptor (VDR; 1:200, cat. no. BS-2987R; Bioss Antibodies; RRID: AB_11058910). VECTASTAIN® Elite® ABC Rabbit IgG Kit (Vector Laboratories, Inc.; RRID: AB_2336817) was used according to manufacturer's instructions. Primary antibodies were incubated overnight at 4˚C. Staining intensity was evaluated by two pathologists independently and scored as +2 (equivalent to positive control), +1 (weaker than positive control), or 0 (unstained) for cytoplasmic and peritumoral stroma. A score of +2 was considered positive.

Co-culture experiments. For indirect co-culture experiments, supernatants from CAFs cultured under hypoxic and normoxic conditions were collected. HT29 cells were then cultured in a medium containing a 1:1 ratio of DMEM supplemented with FBS and the respective CAF-conditioned supernatant.

Treatment with PTHrP and vitamin D. NFs and CAFs were cultured in DMEM supplemented with PBS and PTHrP (1 μg/ml) at 37˚C and 5% CO_2. For vitamin D experiments, CAFs were cultured in DMEM supplemented with 1α,25-dihydroxyvitamin D3 (10 μg/ml) dissolved in dimethyl sulfoxide (DMSO; final DMSO concentration ≤0.5%) at 37˚C and 5% CO_2.

Cell proliferation assay. Cells were seeded in 96-well plates at a density of $1.0x10^3$ cells/well. Cell proliferation was assessed at 24, 48 and 72 h after treatment using 10 μl of Cell Counting Kit-8 (cat. no. CK04; Dojindo Molecular Technologies, Inc.) at 37˚C for 2 h according to the manufacturer's protocol. The association between absorbance measurements and manual cell counting was verified before the experiment. Absorbance was measured at 450 nm.

Cell migration assay. The wound healing assay was used to assess cell migration. Cells were plated in 6-well dishes at $2.0x10^5$ cells/well and cultured to 60-80% confluency. A 200-μl pipette tip was used to create a linear scratch in the cell monolayer. Culture medium was switched to DMEM containing 1% FBS to inhibit cell proliferation. Images were captured using a BZ-X710 microscope (Keyence Corporation) at 0, 24 and 48 h post-scratch and analyzed using ImageJ (version 1.54f; National Institutes of Health) (RRID:SCR_003070). Cell migration was quantified by measuring the mean area between wound edges at three randomly selected locations by an investigator blinded to the experimental conditions.

Drug sensitivity assay. HT29 cells co-cultured with supernatant from normoxia- or hypoxia-cultured CAFs were seeded in 96-well plates at $1.0x10^4$ cells/well for 24 h. Cells were then exposed to varying concentrations of oxaliplatin. Cell viability was evaluated using Cell Counting Kit-8 according to the manufacturer's protocol.

RNA sequencing and analysis. Sample preparation and library construction were performed using the TruSeq stranded mRNA sample preparation kit (Illumina, Inc.) following the manufacturer's protocols. HCT116, HT29 and RKO cell lines were cultured under normoxic (37˚C, 5% CO_2) and hypoxic (37˚C, 1% O_2) conditions. Sequencing was performed on a DNBSEQ-G400 sequencer (MGI Tech Co., Ltd.) in 100-base single-read mode. Adapter sequences were removed using Trimmomatic (version 0.38; RRID:SCR_011848). Cleaned reads were aligned to the hg19 human reference genome using TopHat2 (version 2.1.1; RRID:SCR_013035). Fragments per kilobase of exons per million mapped fragments were calculated using Cufflinks (version 2.2.1; RRID:SCR_014597). Gene Set Variation Analysis was performed using R (version 4.3.2; RRID:SCR_001905). RNA quality and integrity were assessed using the Agilent 2100 Bioanalyzer system. RNA integrity was evaluated by electrophoresis to measure the degree of degradation. Sequencing was performed using the NovaSeq 6000 S1 Reagent Kit v1.5 (200 cycles; cat. no. 20028318; Illumina, Inc.). Final library concentrations were quantified using the KAPA Library Quantification Kit (cat. no. KK4824/D; Roche Diagnostics) by real-time PCR. Libraries were normalized to 2 nM before loading onto the sequencer.

Proteomics analysis. Supernatants from CAFs cultured under hypoxic and normoxic conditions were collected. Total protein was extracted using radioimmunoprecipitation assay buffer containing protease and phosphatase inhibitors (Thermo Fisher Scientific, Inc.). Proteins were processed using nano liquid chromatography-tandem mass spectrometry configured with an Ultimate 3000 Nano LC system, Q-Exactive (Thermo Fisher Scientific, Inc.). Raw data were analyzed using Scaffold 5 (Proteome Software Inc.; RRID:SCR_014345). Ionization mode was positive (nano-ESI with capillary voltage of 1.8 kV). Flow rate was 300 nl/min.

Single-cell RNA sequencing. CAFs cultivated under both hypoxic and normoxic conditions were prepared for single-cell RNA sequencing. Libraries were prepared according to the Chromium Next GEM Single Cell 3'Reagent Kits (version 3.1; 10X Genomics, Inc.) protocols. Sequencing was performed on an Illumina HiSeq X platform. The Cell Ranger pipeline (version 6.1.1; RRID:SCR_017344) was used to generate the data matrix. Raw sequencing reads were mapped to the human reference genome (GRCh 38) using the STAR aligner (RRID:SCR_015899). Data visualization and analysis were performed using Loupe Browser (version 6.0.1; 10X Genomics, Inc.).

Bioinformatics analysis. For Gene Ontology (GO) analysis, the top 100 differentially expressed genes (DEGs) ranked by P-value were analyzed using the Metascape platform

(https://metascape.org; RRID: SCR_016620). Volcano plots and correlation analyses (Pearson's correlation coefficient) were performed using RStudio. Copy Number Variation (CNV) data were obtained from The Cancer Genome Atlas (TCGA) dataset through the cBioPortal platform (RRID:SCR_014555). Gene information and chromosomal locations were obtained from the National Center for Biotechnology Information (NCBI) Gene database (RRID:SCR_002472).

Statistical analysis. Statistical analyses were performed using GraphPad Prism (Dotmatics; RRID: SCR_002798). Data are presented as the mean ± standard deviation from at least three independent experiments. Comparisons between two groups were performed using two-tailed unpaired Student's t-test. For multiple comparisons, one-way analysis of variance followed by Tukey's post-hoc test was used. Correlation analyses were performed using Pearson's correlation coefficient and Spearman's rank correlation coefficient. $P<0.05$ was considered to indicate a statistically significant difference.

Data availability. All RNA and single-cell RNA sequencing data generated in the present study have been deposited in the Gene Expression Omnibus. CNV data from TCGA were accessed through the cBioPortal platform (https://www.cbioportal.org/). Gene information was obtained from the NCBI database (https://www.ncbi.nlm.nih.gov/).

Results

Morphology and immunofluorescence staining of CAFs and NFs. Both CAFs and NFs exhibited a spindle-shaped morphology, but NFs appeared slightly more flattened (Fig. 1A). Immunofluorescence staining revealed that CAFs were positive for α-SMA, while NFs were negative. EpCAM, an epithelial marker, was not detected in either cell type, confirming the successful establishment of CAFs and NFs culture systems (Fig. 1B).

Proliferation of CAFs and NFs under normoxic and hypoxic conditions. Both CAFs and NFs exhibited a significantly enhanced proliferative capacity under hypoxic conditions compared with normoxic conditions ($P<0.05$; Fig. 1C).

Co-culture of CAFs and HT29. HT29 cells cultured with the supernatant from CAFs cultured under both normoxic and hypoxic conditions showed no significant difference in proliferative capacity (Fig. 2A). However, HT29 cells treated with supernatants from hypoxia-conditioned CAFs exhibited a significantly enhanced migratory ability ($P<0.05$; Fig. 2B) and increased resistance to oxaliplatin (cat. no. S1224; Selleck Chemicals) and 5-Fluorouracil (5-FU; cat. no. 16220-14; Nacalai Tesque, Inc.) ($P<0.05$; Fig. 2C), a key chemotherapeutic drug for CRC.

Vitamin D-binding protein (DBP) was significantly increased in the supernatant of hypoxic CAFs. Shotgun proteomic analysis identified 59 proteins in the supernatant of CAFs. Furthermore, a t-test comparing protein levels in the supernatant of CAFs cultured under hypoxic and normoxic conditions identified six proteins with $P<0.01$ and the average value fold change greater than two (Table I). Among these, DBP exhibited the most significant increase.

In a single-cell analysis of CAFs cultured under hypoxic and normoxic conditions, the cells were classified into 15 clusters (Fig. 3A). Clusters exhibiting upregulation of CAF markers were identified. Clusters 2, 5, 6 and 7, characterized by high expression of α-SMA, periostin and HIF-1α, were selected for further analysis (Fig. 3B and C). In addition, examination of our dataset for the expression of CAF marker genes reported by Elyada *et al* (22) revealed that several markers such as FAP and MYL9 were expressed at high levels in clusters 2, 5, 6 and 7 (Fig. S1). These clusters were then re-clustered, and DEGs between hypoxic and normoxic CAFs were identified within each cluster (Fig. 3D). The proportions of hypoxic and normoxic cells in each cluster can be confirmed in Table SI.

GO and Kyoto Encyclopedia of Genes and Genomes pathway analyses revealed that genes upregulated in hypoxic CAFs were markedly enriched in pathways related to ossification, skeletal development and the phosphoinositide 3-kinase-AKT signaling pathway (PI3K-AKT) signaling pathway (Fig. 3E and F).

Identification of PTHrP as a key factor in hypoxic CAFs. Given the critical role of crosstalk between CAFs and tumor cells in the TME, it was aimed to elucidate common hypoxic response mechanisms across the entire TME. By identifying genes whose expression was altered not only in hypoxic CAFs but also in hypoxic CRC cells, the aim was to identify key factors involved in CAF-cancer cell interactions that contribute to tumor progression and drug resistance. Among the upregulated genes in hypoxic CAFs, 59 genes were identified that were also upregulated in hypoxic CRC cell lines (Table SII). From these 59 genes, those strongly associated with vitamin D, bone metabolism and the PI3K-AKT signaling pathway were selected, factors previously identified as crucial through hypoxic CAF secretome analysis and pathway analysis, as candidates for further investigation. Based on these findings, PTHrP was identified as a key factor in hypoxic CAFs and designated as the primary candidate for further analysis.

Effect of PTHrP on NF and effect of PTHrP and vitamin D on CAF. When PTHrP was added to NFs under normoxic conditions, both α-SMA and HIF-1α expression increased (Fig. 4A). In CAFs, PTHrP treatment induced morphological changes similar to those observed in hypoxic CAF, with cells transitioning from a spindle-shaped to a more flattened morphology and forming layered structures (Fig. 4B), along with enhanced proliferation capacity (Fig. 4C). DBP, identified through shotgun analysis of the conditioned medium from hypoxic CAFs, has been reported to reduce tissue vitamin D levels (23), which are known to exert anticancer effects (24). Given that vitamin D has been reported to downregulate PTHrP expression (25), vitamin D was added to the CAF culture medium to investigate possible attenuation of their CAF-like features. Vitamin D treatment led to morphological reversion of CAFs to an NF-like appearance (Fig. 4B), although no significant suppression of proliferation was observed (Fig. 4C).

Immunostaining analysis of DR patterns in patients with CRC. Immunohistochemical analysis of DR patterns

Table I. A total of six proteins with [a]P<0.05 shown by Student's t-test between the two groups and a ratio of the mean greater than 2-fold.

MS/MS View: Identified Proteins (CAF)	n1	n2	n3	h1	h2	h3	P-value	n/h ratio
Vitamin D-binding protein	5	6	5	9	12	13	0.0152	0.47
Delta-globin B2 variant (Fragment)	2	2	2	0	1	1	0.0286	3
Mutant hemoglobin alpha 2 globin chain	6	5	5	4	1	0	0.0417	3.2
Collagen alpha-1(I)	3	2	4	1	1	0	0.0178	4.5
Collagen alpha-2(I) chain	3	3	4	1	0	0	0.0016	10
Fibronectin 1, isoform CRA_n	3	7	6	0	1	0	0.0224	16

[a]P<0.05 by T-test between the two groups and ratio of means >2-fold.

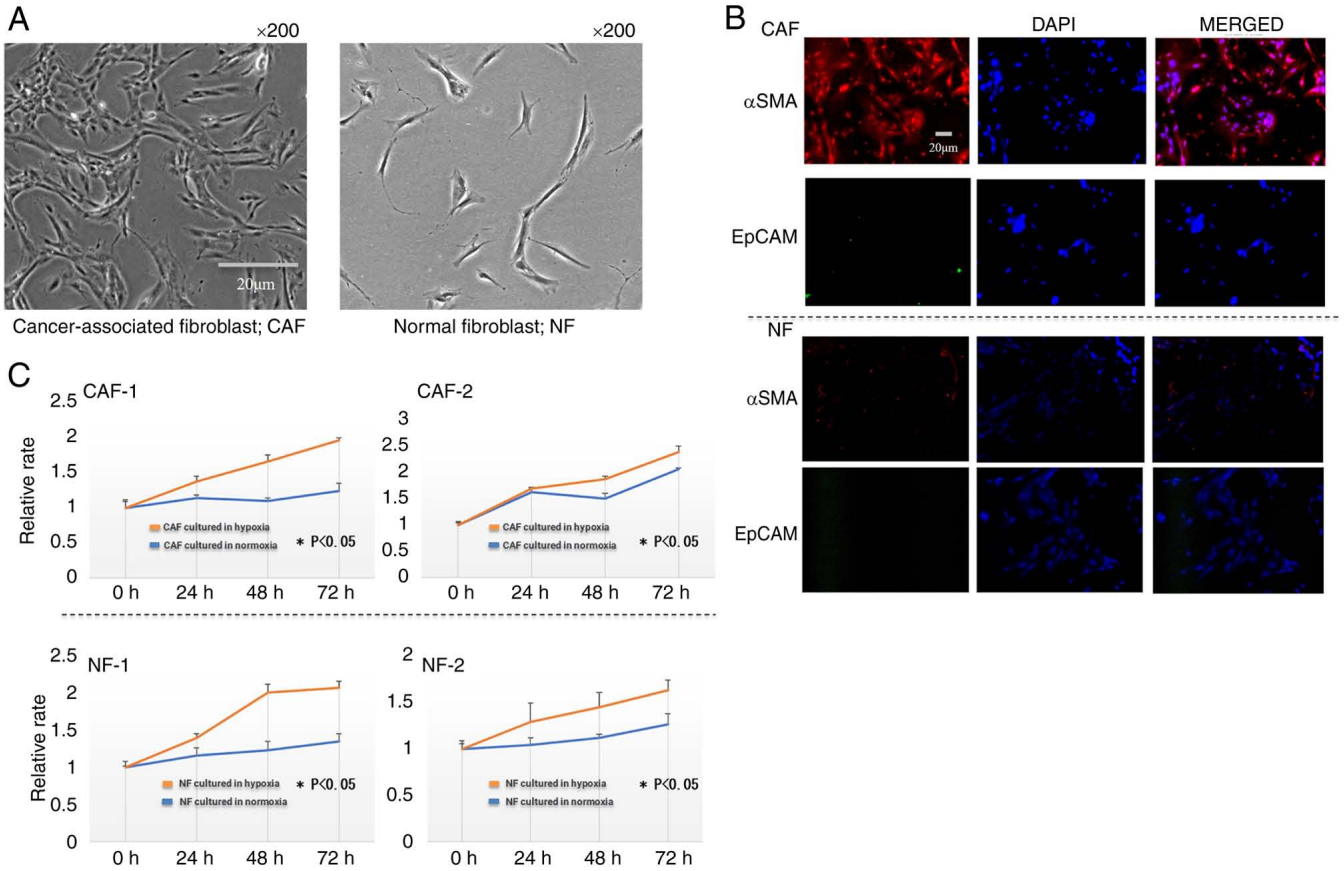

Figure 1. Primary culture and hypoxic culture of fibroblasts. (A) CAF and NF morphology. (B) CAF and NF observed by immunofluorescence staining. (C) Proliferation assay of CAF and NF under both normoxic and hypoxic conditions. The data are shown as the mean ± SD of three independent experiments. *P<0.05, Student's t-test. CAF, cancer-associated fibroblast; NF, normal fibroblast.

(16 mature, nine immature) revealed significantly higher expression of HIF-1α and periostin, one of the reported CAF markers, in the immature group, indicating that these tumors were exposed to a more hypoxic microenvironment (Fig. 5A; Table II). To perform a more detailed analysis, an expanded cohort of 59 cases (43 mature, 16 immature) was examined. In this cohort, the immature group showed significantly higher PTHrP expression in both cytoplasm of tumor cells at the invasive front and the surrounding stromal areas. Since RAS mutation has been reported as one of the upstream regulators of PTHrP (25), the results of genetic testing performed on tumor tissue samples were also analyzed. Among the 59 cases, 43 had undergone testing for RAS and B-Raf proto-oncogene mutations and microsatellite instability status, with KRAS mutations found in 20 cases and neuroblastoma RAS viral oncogene homolog mutation in one case (Table SIII) and MSI testing results showed 0% (0/13) MSI-H cases in the immature DR group and 10.0% (3/30) in the mature DR group, comparable to the reported 5-10% prevalence in general CRC populations. This suggests that the current cohort is not uniquely biased toward MSS cases.

Table II. Correlation between desmoplastic reaction and clinicopathological factors including HIF-1α and periostin expression in CRC samples.

Variable	Desmoplastic reaction		P-value
	Immature (n=9)	Mature (n=16)	
Patient characteristics			
Age at surgery (years), [IQR]	71.2 [46-88]	67.9 [56-84]	0.394
Male sex	5 (55.6%)	7 (43.8%)	0.691
Tumor characteristics			
Location (right/left)	3/6	5/11	0.915
T stage (1-2/3-4)	0/9	2/14	0.520
N stage (0/1-3)	3/6	8/8	0.677
Venous invasion	5 (55.6%)	10 (62.5%)	0.734
Lymphatic invasion	4 (44.4%)	8 (50.0%)	0.789
Perineural invasion	6 (66.7%)	7 (43.8%)	0.411
HIF-1α high expression	6 (66.7%)	3 (18.8%)	0.0308
Periostin high expression	8 (88.9%)	7 (43.8%)	0.0405

Values are given as n or n (%) unless otherwise noted. IQR, interquartile range; HIF-1α, hypoxia-inducible factor-1α; CRC, colorectal cancer.

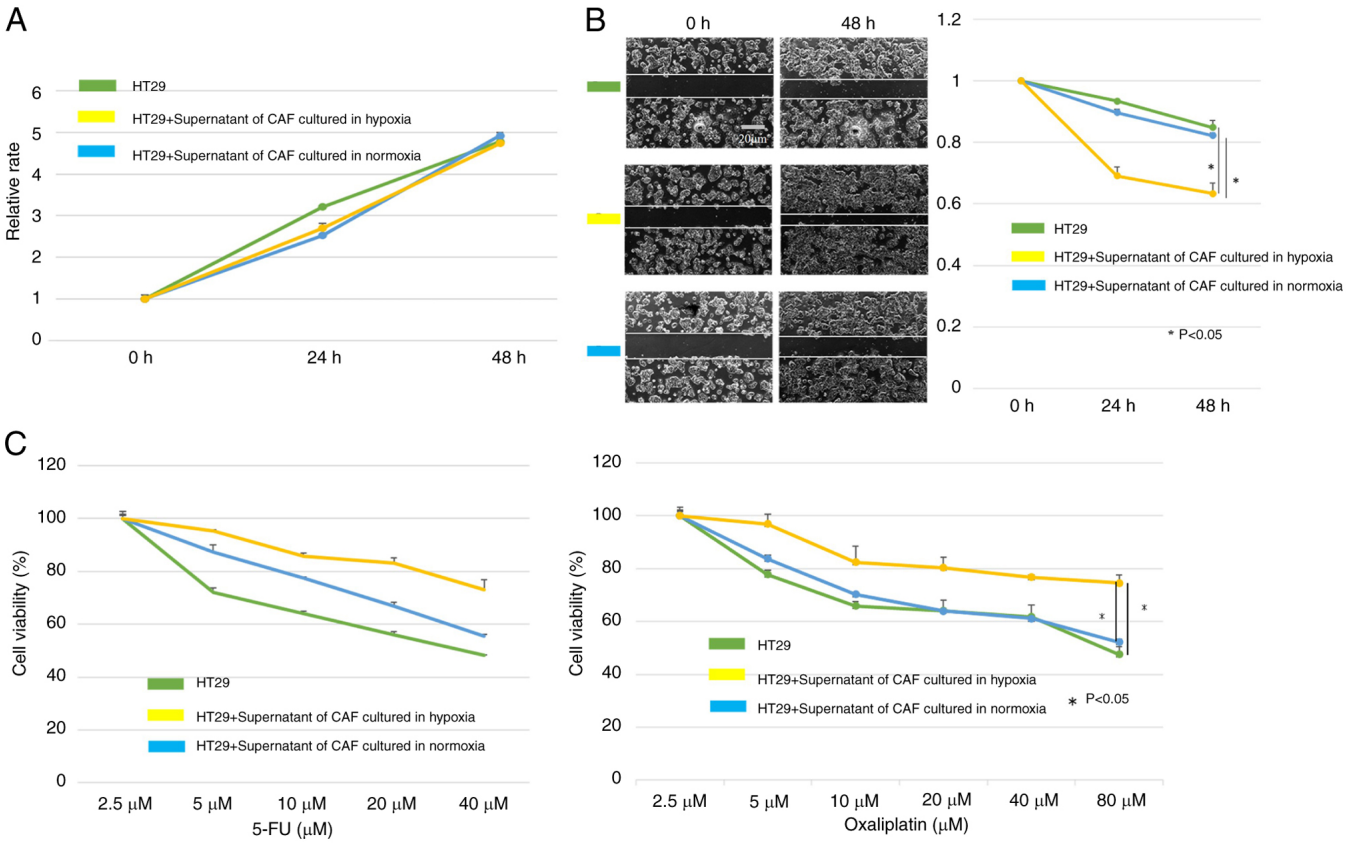

Figure 2. Investigation by co-culture of CAF supernatant and HT29. (A) Proliferation assay using HT29 and HT29 co-cultured with supernatant of CAF cultured in both normoxia and hypoxia. (B) Cell migration assay using both HT29 and HT29 co-cultured with supernatant of CAF cultured in both normoxia and hypoxia. (C) Oxaliplatin and 5-FU sensitivity assay using both HT29 and HT29 co-cultured with supernatant of CAF cultured in both normoxia and hypoxia. The data are shown as the mean ± SD of three independent experiments. *P<0.05, Student's t-test. CAF, cancer-associated fibroblast; 5-FU, 5-Fluorouracil.

RAS mutations were found to be significantly more frequent in the immature group (Fig. 5B; Table III). Subgroup analysis based on PTHrP expression levels in both the cancer cells at the invasive front and the surrounding stroma showed

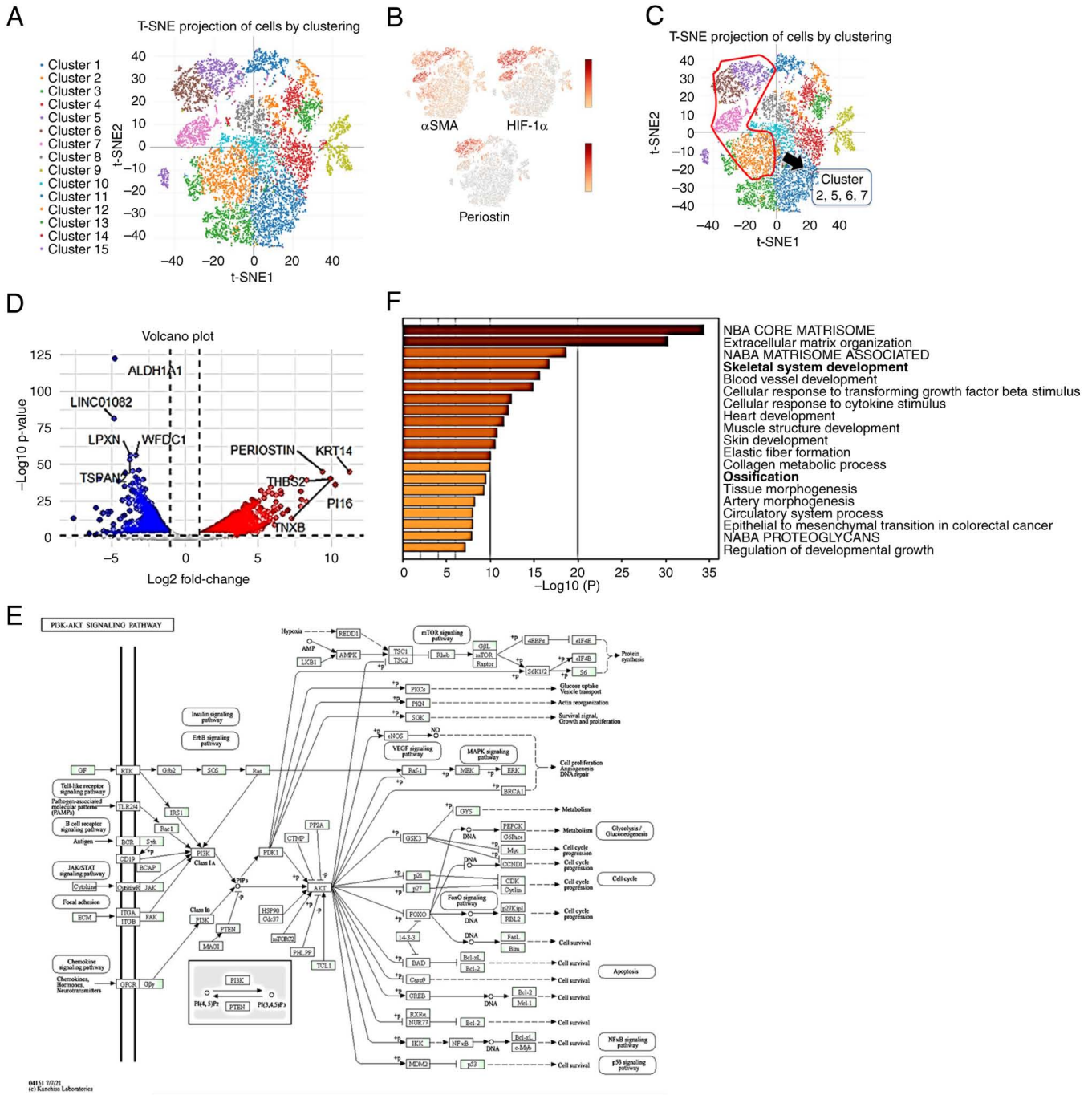

Figure 3. Single-cell RNA sequencing of human CAF and generation of data matrix. (A) CAF divided into 15 clusters. (B) CAF gene expression of α-SMA, HIF-1α and periostin. (C) Selected clusters with high expression of α-SMA, HIF-1α and periostin. (D) Volcano plots created from DEGs of cluster 2, 5, 6 and 7. (E) Gene list was generated from DEGs and KEGG pathway analysis was performed. (F) Gene list was generated from DEGs and GO analysis was performed. CAF, cancer-associated fibroblast; α-SMA, α-smooth muscle actin; HIF-1α, hypoxia-inducible factor-1α; DEG, differentially expressed gene; GO, Gene Ontology; KEGG, Kyoto Encyclopedia of Genes and Genomes.

a positive correlation between PTHrP expression and RAS mutation status (Tables IV and SII).

Correlation between copy number variations of PTHrP and KRAS. To further investigate the association between PTHrP expression and RAS mutation observed in tumor tissue, the relationship between PTHrP and KRAS was analyzed using public datasets. Both PTHrP and KRAS are located on chromosome 12. Analysis of CNVs in patients with CRC using TCGA data revealed a significant positive correlation between KRAS and PTHrP copy number (R=0.92; P<0.001; Fig. 5C). Similar trends were observed across multiple cancer types (Fig. 5D).

Furthermore, copy number correlations were analyzed for other known driver genes located on chromosome 12, CDK4 and MDM2, and a very strong positive correlation was found between them (Spearman's r=0.91; $P=5.17x10^{-196}$; Fig. S2A). Strong copy number correlations were also observed between VDR, which is located on the same chromosome, and both PTHrP (Fig. S2B) and KRAS

Table III. Correlation between desmoplastic reaction and clinicopathological factors including PTHrP expression or genetic testing in CRC samples.

Variable	Desmoplastic reaction		P-value
	Immature (n=16)	Mature (n=43)	
Patiet characteristics			
Age at surgery (years), [IQR]	69.9 [46-88]	71.7 [40-87]	0.578
Male sex	5 (45.5%)	21 (48.8%)	0.255
Tumor characteristics			
Location (right/left)	8/8	17/26	0.559
T stage (1-2/3-4)	0/16	2/41	0.256
N stage (0/1-3)	6/10	25/18	0.241
Venous invasion	11 (68.8%)	23 (53.5%)	0.380
Lymphatic invasion	7 (43.8%)	18 (41.9%)	0.976
Perineural invasion	8 (50.0%)	12 (27.9%)	0.132
PTHrP high expression	12 (75.0%)	13 (30.2%)	0.0029
Genetic testing performed	13 (81.3%)	30 (69.8%)	-
RAS mutation	10/13 (76.9%)	11/30 (36.7%)	0.0217
BRAF mutation status	0/13 (0%)	3/30 (10.0%)	0.542
MSI-H cases, n (%)	0/13 (0%)	3/30 (10.0%)	0.542

Values are given as n or n (%) unless otherwise noted. IQR, interquartile range; PTHrP, parathyroid hormone-related protein; CRC, colorectal cancer.

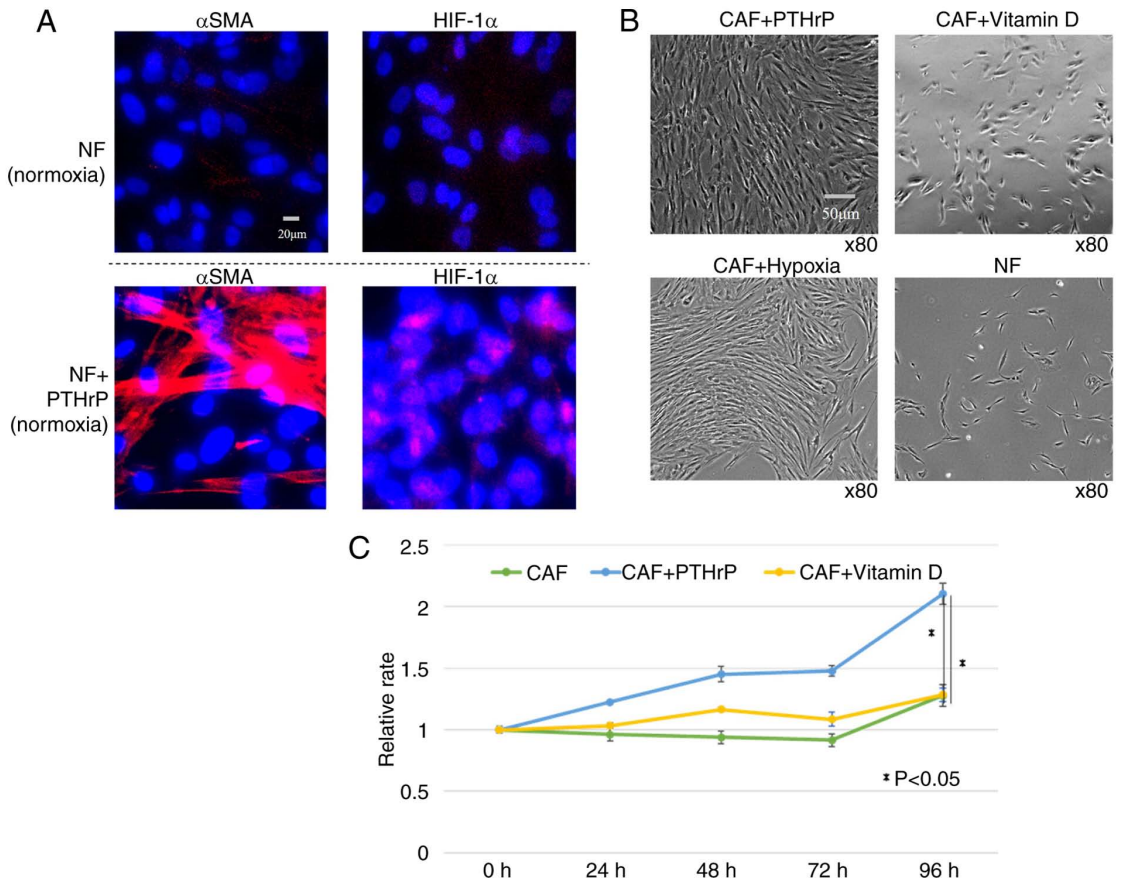

Figure 4. Selection of PTHrP. PTHrP effects on NF and the influence of PTHrP and vitamin D on CAF. (A) Immunofluorescence staining of NF with PTHrP. (B) Morphology of CAF supplemented with PTHrP or vitamin D. (C) Proliferation assay using both CAF and CAF supplemented with PTHrP or vitamin D. The data are shown as the mean ± SD of three independent experiments. *P<0.05, Student's t-test. PTHrP, parathyroid hormone-related protein; NF, normal fibroblast; CAF, cancer-associated fibroblast.

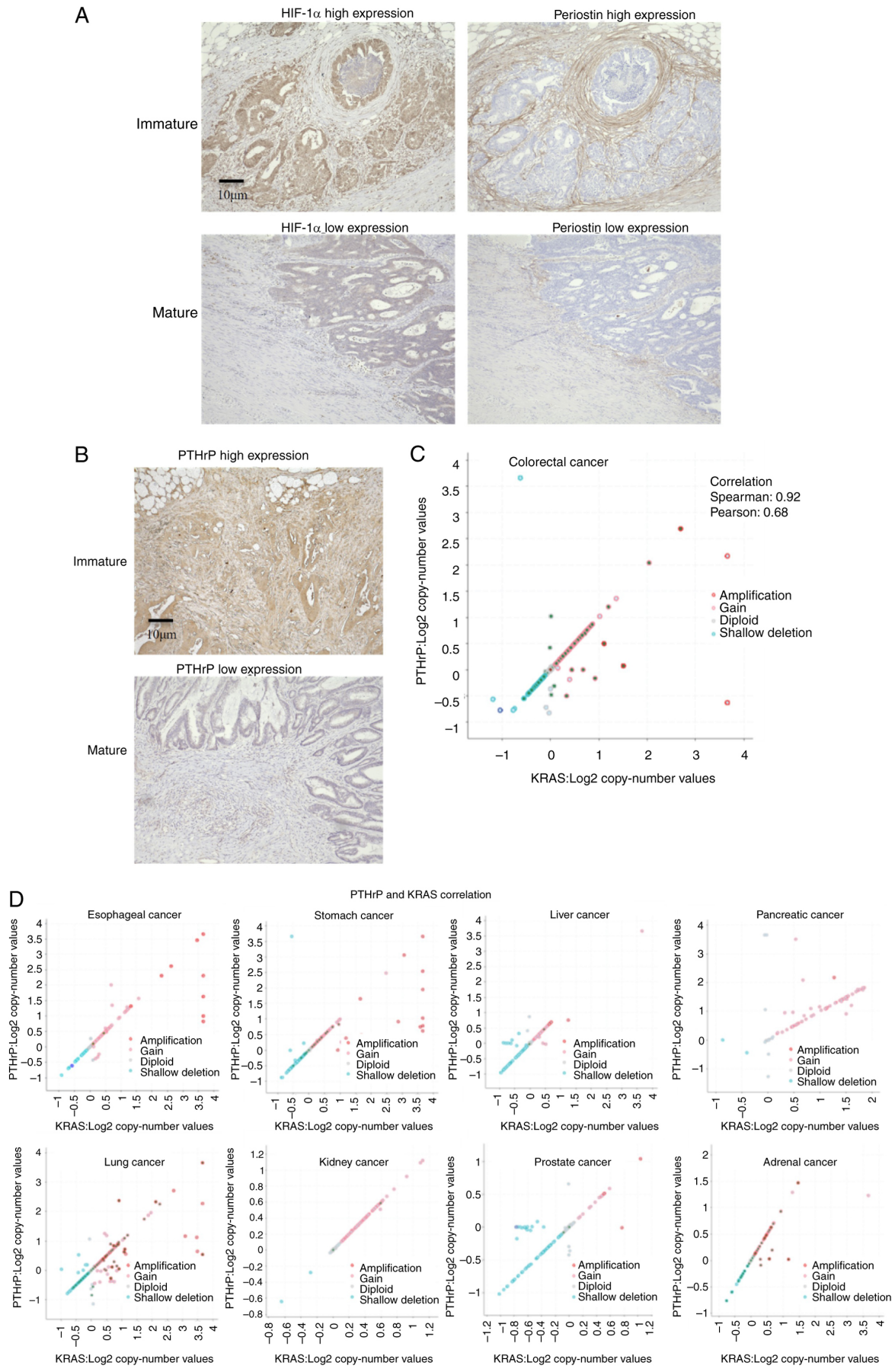

Figure 5. Examination of interrelationships among PTHrP, vitamin D and RAS. (A and B) Representative image of immunohistochemical staining of CRC tissue for HIF1-α, periostin, PTHrP and VDR. (C) Correlation of copy numbers in CRC for PTHrP and KRAS. (D) Correlation of copy numbers in various cancers for PTHrP and KRAS. PTHrP, parathyroid hormone-related protein; RAS, rat sarcoma oncogene; CRC, colorectal cancer; HIF-1α, hypoxia-inducible factor-1α; VDR, vitamin D receptor; KRAS, Kirsten rat sarcoma viral oncogene homolog.

Table IV. A subgroup analysis examining the correlation between clinicopathological factors and two groups divided based on high and low expression of PTHrP.

	PTHrP expression		
Variable	Low (n=34)	High (n=25)	P-value
Tumor characteristics			
Location (right/left)	14/20	11/14	0.828
T stage (1-2/3-4)	2/32	0/25	0.503
N stage (0/1-3)	18/16	13/12	0.943
Venous invasion	18 (52.9%)	16 (64.0%)	0.435
Lymphatic invasion	15 (44.1%)	11 (44.0%)	0.993
Perineural invasion	11 (32.4%)	9 (36.0%)	0.788
Genetic testing performed	22 (64.7%)	21 (84.0%)	-
RAS mutation	7/22 (31.8%)	14/21 (66.7%)	0.0337

Values are given as n or n (%) unless otherwise noted. IQR, interquartile range; PTHrP, parathyroid hormone-related protein.

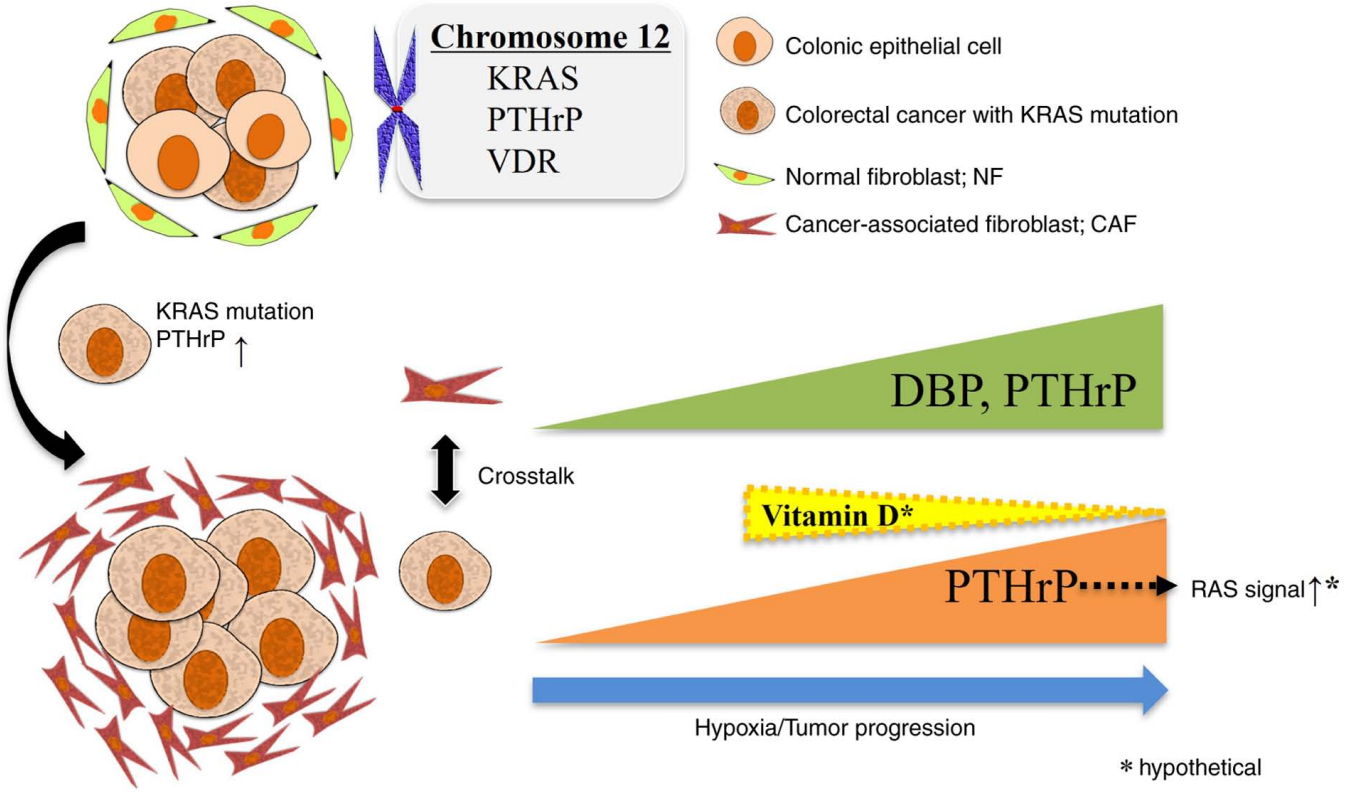

Figure 6. Graphic abstract. Hypoxic CAFs enhance tumor growth through PTHrP signaling and DBP secretion, reducing local vitamin D levels in the peritumoral region. The observed correlation between PTHrP expression in tumor cells and RAS signaling suggests that the PTHrP-vitamin D-RAS axis may play a key role in the tumor microenvironment. CAF, cancer-associated fibroblast; PTHrP, parathyroid hormone-related protein; DBP, vitamin D-binding protein; RAS, rat sarcoma oncogene.

(Fig. S2C; PTHrP, Spearman's r=0.77; P=7.13x10^{-106}; KRAS, Spearman's r=0.78; P=5.90x10^{-111}). These results support the possibility that the co-amplification of PTHrP and KRAS is a passenger event associated with regional chromosomal gains on chromosome 12, and also suggest potential involvement of other functional relationships, such as vitamin D signaling through VDR.

Discussion

In the present study, the focus was on the hypoxic microenvironment, which is known to promote cancer progression, and the aim was to elucidate the phenotypic changes of CAFs under hypoxia and their underlying mechanisms. The results demonstrated that hypoxia significantly enhanced the

proliferative capacity of both CAFs and NFs. Furthermore, the conditioned medium from hypoxia-cultured CAFs significantly promoted chemoresistance and migratory ability in CRC cell lines.

CAFs are a major component of the stromal cell population within the TME (1), and their characteristics are notably influenced by crosstalk with tumor cells (5). In CRC, the DR classification, categorized as immature, intermediate, or mature, has been used as a prognostic indicator (8). Since CAFs constitute the tumor stroma and interact closely with cancer cells, evaluating CAF activity and the stromal status using the DR classification is considered important. CAFs release various factors that modify the TME, and these changes are likely reflected in the DR classification.

Hypoxia, a common feature observed across numerous solid tumors (10), influences critical aspects of cancer biology, including cellular invasion, distant metastasis and regulation of cell death processes (11). In the present study, a marked increase in DBP was observed in the conditioned medium of hypoxia-cultured CAFs, whereas collagen and fibronectin levels were reduced. The decreased levels of these extracellular matrix (ECM) components may be explained by HIF-1α upregulation promoting ECM degradation, consistent with the current finding that HIF-1α-high CAF clusters exhibited increased MMP2 expression. DBP binds to vitamin D metabolites and transports them to organs such as the liver, thereby reducing free vitamin D concentrations (23). As a result, increased DBP levels in tissue can decrease local vitamin D availability.

Single-cell analysis revealed enrichment of bone metabolism-related genes in hypoxic CAFs. Bone metabolism-related factors have garnered attention as therapeutic targets in solid tumors (26,27), and vitamin D, in particular, is known to exert suppressive effects on cancer. Increased total vitamin D intake has been reported to be associated with a reduced risk of early-onset CRC and its precursors (24). These findings suggest that the vitamin D-related network is one of the critical factors directly associated with cancer aggressiveness.

In the current study, the focus was on PTHrP as a factor through which hypoxic CAFs may promote tumor malignancy. Transcription of the *PTHrP* gene is suppressed by $1,25(OH)_2D$ and hypocalcemic vitamin D analogs, and this suppression may help alleviate hypercalcemia caused by tumor-derived overproduction of PTHrP (25). Moreover, *PTHrP* gene activation is associated with malignant transformation in normal mammalian cells, with Ras and p53 identified as key upstream regulators of *PTHrP* transcription (28).

In CRC, frequent abnormalities have been reported in major intracellular signaling pathways, including those involving Ras and p53 (29). In some patients with gastrointestinal cancers showing p53 immunoreactivity, vitamin D supplementation has been reported to reduce the risk of recurrence or death (30).

PTHrP was selected as a key factor in CAFs under hypoxic conditions. PTHrP has also been reported as one of the major causes of hypercalcemia in cancer-bearing states (31). Since vitamin D and PTHrP are closely involved in cancer physiology *in vivo*, it is strongly suggested that they may also influence CAFs in the TME.

Immunohistochemical analysis of DR-classified samples showed that the positivity rates of HIF-1α, a hypoxia marker (32), and periostin, which is also considered a CAF marker (33), were higher in the immature group, suggesting that this group is exposed to a more severe hypoxic environment. PTHrP expression was positively correlated with the prognostically poor immature type, confirming its association with hypoxia.

RAS mutations in tumor cells are important factors that influence the biological behavior of CRC (34), and RAS-mutant CRCs exhibit distinct characteristics, making the development of novel therapies highly anticipated (35). The RAS mutation rate was elevated in both the immature type of the DR classification and the high-PTHrP expression group. These findings suggest a potential association between KRAS-mutant CRC and both the immature stromal type and high PTHrP expression.

In PCa, where KRAS mutations are frequently observed, DR caused by CAFs is prominent, and the resulting dense stroma inhibits angiogenesis, leading to hypoxic regions within the tumor (36). In addition to KRAS amplification, amplification of the *PTHLH* gene, which encodes PTHrP, has also been observed in patients with PCa, and PTHrP has been reported to promote tumor growth and metastasis (37).

In the present study, correlation analysis across various cancer types revealed a strong association between the copy numbers of KRAS and PTHrP. Both KRAS and PTHrP are located on chromosome 12.

In summary, CAFs under hypoxic conditions exhibit tumor-promoting properties, and single-cell analysis revealed that PTHrP is one of the key factors involved. In addition, hypoxic CAFs increase the secretion of DBP, leading to a reduction in the local concentration of vitamin D around the tumor. Similar to the known relationship between PTH and vitamin D, a potential interaction between PTHrP and vitamin D was also suggested. Immunohistochemical analysis indicated that CRC tissues with high PTHrP expression are exposed to a more hypoxic environment, and these features were also strongly correlated with KRAS mutations. Furthermore, analysis of public datasets showed a strong correlation between the copy numbers of PTHrP and KRAS, suggesting that the PTHrP-vitamin D-RAS axis may be a key regulatory pathway involving CAFs.

One limitation of the present study is that vitamin D levels were not evaluated, as quantification of vitamin D within tissue samples is technically challenging. The concentration of vitamin D in resected CRC specimens is likely influenced by various factors, including the absorption status of intestinal epithelium at the time of surgery and the circulating levels of vitamin D. Therefore, it is challenging to accurately assess tissue vitamin D levels and their impact on CAFs.

These findings suggest a potential PTHrP-vitamin D-RAS axis in the function of CAFs, in which hypoxia-induced PTHrP expression in tumor cells is associated with enhanced RAS signaling. This axis may provide new insights into CAF biology and TME interactions (Fig. 6).

The present study has several limitations that should be considered. Fluorescence images were evaluated based on

qualitative comparisons rather than quantitative measurements. This approach was chosen because the cultured CAFs and NFs were not 100% pure, and contaminating cell populations could limit the reliability of quantitative analysis. Additionally, structural differences between tissue samples and uneven antibody staining made quantitative fluorescence measurements technically challenging and potentially misleading.

Due to technical constraints, an indirect co-culture system was employed in the present study, which limited the assessment of direct CAF-tumor cell interaction pathways. This may explain why our proteomic analysis did not reveal clear increases in proliferation-related proteins despite observing enhanced migration. Future studies employing direct co-culture systems and pathway blockade assays using specific inhibitors would provide valuable insights into the cytokine profiling and proliferation signaling cascades involved in CAF-tumor cell interactions.

While focus was addressed on HIF-1α as the primary hypoxic response indicator, other common canonical HIF targets such as VEGF, CA9 and GLUT1 were not comprehensively assessed. Single-cell analysis showed that clusters with high HIF-1α expression also exhibited increased VEGF and GLUT1 expression, while CA9 showed no marked increase. However, functional validation of these targets and their roles in the hypoxic CAF phenotype was not performed in the present study. Additionally, whether PTHrP is a direct transcriptional target of HIF-1α in CRC remains unclear and requires further investigation through chromatin immunoprecipitation-sequencing or promoter assays. Future studies should comprehensively evaluate the expression and functional significance of canonical hypoxia regulators in CAFs and validate the direct transcriptional regulation of PTHrP by HIF-1α.

Acknowledgements

Not applicable.

Funding

No funding was received.

Availability of data and materials

The data generated in the present study may be found in the Japan ProteOme STandard Repository under accession number JPST004147 or at the following URL: https://repository.jpostdb.org/entry/JPST004147; in the DDBJ Sequence Read Archive (DRA) under accession numbers DRA023624 and DRA023649 or at the following URL (https://ddbj.nig.ac.jp/search); in the NCBI SRA database under accession numbers DRA023624 and DRA023649 or at the following URL: (https://www.ncbi.nlm.nih.gov/sra/?term=DRA023624 and https://www.ncbi.nlm.nih.gov/sra/?term=DRA023649).

Authors' contributions

SN and MU substantially contributed to the study conceptualization and design. HK, MO, CK, NT and MTa contributed to data acquisition. SN significantly contributed to data analysis and interpretation, and manuscript drafting. SN and MU critically revised the manuscript for important intellectual content. SN and MU confirm the authenticity of all the raw data. All authors read and approved the final version of the manuscript and agreed to be accountable for all aspects of the work.

Ethics approval and consent to participate

The present study was approved by the Human Ethics Review Committee of the Graduate School of Medicine, University of Osaka (approval nos. 15144 and 19020; Suita, Japan). Written informed consent was obtained from all patients for the use of their tissue samples for research purposes, including primary cell isolation.

Patient consent for publication

Not applicable.

Competing interests

The authors declare that they have no competing interests.

References

1. Luo H, Xia X, Huang LB, An H, Cao M, Kim GD, Chen HN, Zhang WH, Shu Y, Kong X, *et al*: Pan-cancer single-cell analysis reveals the heterogeneity and plasticity of cancer-associated fibroblasts in the tumor microenvironment. Nat Commun 13: 6619, 2022.
2. Mhaidly R and Mechta-Grigoriou F: Role of cancer-associated fibroblast subpopulations in immune infiltration, as a new means of treatment in cancer. Immunol Rev 302: 259-272, 2021.
3. Chen Y, McAndrews KM and Kalluri R: Clinical and therapeutic relevance of cancer-associated fibroblasts. Nat Rev Clin Oncol 18: 792-804, 2021.
4. Broz MT, Ko EY, Ishaya K, Xiao J, De Simone M, Hoi XP, Piras R, Gala B, Tessaro FHG, Karlstaedt A, *et al*: Metabolic targeting of cancer associated fibroblasts overcomes T-cell exclusion and chemoresistance in soft-tissue sarcomas. Nat Commun 15: 2498, 2024.
5. Wu F, Yang J, Liu J, Wang Y, Mu J, Zeng Q, Deng S and Zhou H: Signaling pathways in cancer-associated fibroblasts and targeted therapy for cancer. Signal Transduct Target Ther 6: 218, 2021.
6. Ueno H, Kajiwara Y, Ajioka Y, Sugai T, Sekine S, Ishiguro M, Takashima A and Kanemitsu Y: Histopathological atlas of desmoplastic reaction characterization in colorectal cancer. Jpn J Clin Oncol 51: 1004-1012, 2021.
7. Sandberg TP, Stuart MPME, Oosting J, Tollenaar RAEM, Sier CFM and Mesker WE: Increased expression of cancer-associated fibroblast markers at the invasive front and its association with tumor-stroma ratio in colorectal cancer. BMC Cancer 19: 284, 2019.
8. Hu Q, Wang Y, Yao S, Mao Y, Liu L, Li Z, Chen Y, Zhang S, Li Q, Zhao Y, *et al*: Desmoplastic reaction associates with prognosis and adjuvant chemotherapy response in colorectal cancer: A multicenter retrospective study. Cancer Res Commun 3: 1057-1066, 2023.
9. Akimoto N, Väyrynen JP, Zhao M, Ugai T, Fujiyoshi K, Borowsky J, Zhong R, Haruki K, Arima K, Lau MC, *et al*: Desmoplastic reaction, immune cell response, and prognosis in colorectal cancer. Front Immunol 13: 840198, 2022.
10. Sueyama T, Kajiwara Y, Mochizuki S, Shimazaki H, Shinto E, Hase K and Ueno H: Periostin as a key molecule defining desmoplastic environment in colorectal cancer. Virchows Arch 478: 865-874, 2021.
11. Wilson WR and Hay MP: Targeting hypoxia in cancer therapy. Nat Rev Cancer 11: 393-410, 2011.
12. Chi JT, Wang Z, Nuyten DS, Rodriguez EH, Schaner ME, Salim A, Wang Y, Kristensen GB, Helland A, Børresen-Dale AL, *et al*: Gene expression programs in response to hypoxia: Cell type specificity and prognostic significance in human cancers. PLoS Med 3: e47, 2006.

13. Uemura M, Yamamoto H, Takemasa I, Mimori K, Hemmi H, Mizushima T, Ikeda M, Sekimoto M, Matsuura N, Doki Y and Mori M: Jumonji domain containing 1A is a novel prognostic marker for colorectal cancer: In vivo identification from hypoxic tumor cells. Clin Cancer Res 16: 4636-446, 2010.
14. Uemura M, Yamamoto H, Takemasa I, Mimori K, Mizushima T, Ikeda M, Sekimoto M, Doki Y and Mori M: Hypoxia-inducible adrenomedullin in colorectal cancer. Anticancer Res 31: 507-514, 2011.
15. Noda T, Yamamoto H, Takemasa I, Yamada D, Uemura M, Wada H, Kobayashi S, Marubashi S, Eguchi H, Tanemura M, *et al*: PLOD2 induced under hypoxia is a novel prognostic factor for hepatocellular carcinoma after curative resection. Liver Int 32: 110-118, 2012.
16. Yamamoto H, Tei M, Uemura M, Takemasa I, Uemura Y, Murata K, Fukunaga M, Ohue M, Ohnishi T, Ikeda K, *et al*: Ephrin-A1 mRNA is associated with poor prognosis of colorectal cancer. Int J Oncol 42: 549-555, 2013.
17. Wada H, Yamamoto H, Kim C, Uemura M, Akita H, Tomimaru Y, Hama N, Kawamoto K, Kobayashi S, Eguchi H, *et al*: Association between ephrin-A1 mRNA expression and poor prognosis after hepatectomy to treat hepatocellular carcinoma. Int J Oncol 45: 1051-1058, 2014.
18. Munakata K, Uemura M, Takemasa I, Ozaki M, Konno M, Nishimura J, Hata T, Mizushima T, Haraguchi N, Noura S, *et al*: SCGB2A1 is a novel prognostic marker for colorectal cancer associated with chemoresistance and radioresistance. Int J Oncol 44: 1521-1528, 2014.
19. Kawai K, Uemura M, Munakata K, Takahashi H, Haraguchi N, Nishimura J, Hata T, Matsuda C, Ikenaga M, Murata K, *et al*: Fructose-bisphosphate aldolase A is a key regulator of hypoxic adaptation in colorectal cancer cells and involved in treatment resistance and poor prognosis. Int J Oncol 50: 525-534, 2017.
20. Schwörer S, Cimino FV, Ros M, Tsanov KM, Ng C, Lowe SW, Carmona-Fontaine C and Thompson CB: Hypoxia potentiates the inflammatory fibroblast phenotype promoted by pancreatic cancer Cell-derived cytokines. Cancer Res 83: 1596-1610, 2023.
21. Hashiguchi Y, Muro K, Saito Y, Ito Y, Ajioka Y, Hamaguchi T, Hasegawa K, Hotta K, Ishida H, Ishiguro M, *et al*: Japanese society for cancer of the colon and rectum (JSCCR) guidelines 2019 for the treatment of colorectal cancer. Int J Clin Oncol 25: 1-42, 2020.
22. Elyada E, Bolisetty M, Laise P, Flynn WF, Courtois ET, Burkhart RA, Teinor JA, Belleau P, Biffi G, Lucito MS, *et al*: Cross-species single-cell analysis of pancreatic ductal adenocarcinoma reveals antigen-presenting cancer-associated fibroblasts. Cancer Discov 9: 1102-1123, 2019.
23. Bouillon R, Schuit F, Antonio L and Rastinejad F: Vitamin D binding protein: A historic overview. Front Endocrinol (Lausanne) 10: 910, 2019.
24. Kim H, Lipsyc-Sharf M, Zong X, Wang X, Hur J, Song M, Wang M, Smith-Warner SA, Fuchs C, Ogino S, *et al*: Total vitamin d intake and risks of Early-onset colorectal cancer and precursors. Gastroenterology 161: 1208-1217.e9, 2021.
25. Goltzman D, White J and Kremer R: Studies of the effects of 1, 25-dihydroxyvitamin D on skeletal and calcium homeostasis and on inhibition of tumor cell growth. J Steroid Biochem Mol Biol 76: 43-47, 2001.
26. Yang C, Tian Y, Zhao F, Chen Z, Su P, Li Y and Qian A: Bone microenvironment and osteosarcoma metastasis. Int J Mol Sci 21: 6985, 2020.
27. Clézardin P, Coleman R, Puppo M, Ottewell P, Bonnelye E, Paycha F, Confavreux CB and Holen I: Bone metastasis: Mechanisms, therapies, and biomarkers. Physiol Rev 101: 797-855, 2021.
28. Motokura T, Endo K, Kumaki K, Ogata E and Ikeda K: Neoplastic transformation of normal rat embryo fibroblasts by a mutated p53 and an activated ras oncogene induces parathyroid hormone-related peptide gene expression and causes hypercalcemia in nude mice. J Biol Chem 270: 30857-30861, 1995.
29. Li XL, Zhou J, Chen ZR and Chng WJ: P53 mutations in colorectal cancer-molecular pathogenesis and pharmacological reactivation. World J Gastroenterol 21: 84-93, 2015.
30. Kanno K, Akutsu T, Ohdaira H, Suzuki Y and Urashima M: Effect of Vitamin D supplements on relapse or death in a p53-Immunoreactive subgroup with digestive tract cancer: Post hoc analysis of the AMATERASU randomized clinical trial. JAMA Netw Open 6: e2328886, 2023.
31. Mundy GR and Edwards JR: PTH-related peptide (PTHrP) in hypercalcemia. J Am Soc Nephrol 19: 672-675, 2008.
32. Zhao M, Wang S, Zuo A, Zhang J, Wen W, Jiang W, Chen H, Liang D, Sun J and Wang M: HIF-1α/JMJD1A signaling regulates inflammation and oxidative stress following hyperglycemia and Hypoxia-induced vascular cell injury. Cell Mol Biol Lett 26: 40, 2021.
33. Yang Y, Wu J, Zhu H, Shi X, Liu J, Li Y and Wang M: Effect of hypoxia-HIF-1α-periostin axis in thyroid cancer. Oncol Rep 51: 57, 2024.
34. Kerk SA, Papagiannakopoulos T, Shah YM and Lyssiotis CA: Metabolic networks in mutant KRAS-driven tumours: Tissue specificities and the microenvironment. Nat Rev Cancer 21: 510-525, 2021.
35. Zhu G, Pei L, Xia H, Tang Q and Bi F: Role of oncogenic KRAS in the prognosis, diagnosis and treatment of colorectal cancer. Mol Cancer 20: 143, 2021.
36. Brown BA, Myers PJ, Adair SJ, Pitarresi JR, Sah-Teli SK, Campbell LA, Hart WS, Barbeau MC, Leong K, Seyler N, *et al*: A Histone Methylation-MAPK signaling axis drives durable Epithelial-mesenchymal transition in hypoxic pancreatic cancer. Cancer Res 84: 1764-180, 2024.
37. Pitarresi JR, Norgard RJ, Chiarella AM, Suzuki K, Bakir B, Sahu V, Li J, Zhao J, Marchand B, Wengyn MD, *et al*: PTHrP drives pancreatic cancer growth and metastasis and reveals a new therapeutic vulnerability. Cancer Discov 11: 1774-1791, 2021.